Ag29(BDT)12(TPP)4: A Tetravalent Nanocluster

ARTICLE *in* JOURNAL OF THE AMERICAN CHEMICAL SOCIETY · JUNE 2015

Impact Factor: 12.11 · DOI: 10.1021/jacs.5b04547 · Source: PubMed

JACS
JOURNAL OF THE AMERICAN CHEMICAL SOCIETY

Article

pubs.acs.org/JACS

$Ag_{29}(BDT)_{12}(TPP)_4$: A Tetravalent Nanocluster

Lina G. AbdulHalim,[†] Megalamane S. Bootharaju,[†] Qing Tang,[‡] Silvano Del Gobbo,[†] Rasha G. AbdulHalim,[§] Mohamed Eddaoudi,[§] De-en Jiang,[‡] and Osman M. Bakr*[,†]

[†]Division of Physical Sciences and Engineering, Solar and Photovoltaics Engineering Research Center, King Abdullah University of Science and Technology (KAUST), Thuwal 23955-6900, Saudi Arabia

[‡]Department of Chemistry, University of California, Riverside, California 92508, United States

[§]Functional Materials Design, Discovery and Development Research Group (FMD3), Advanced Membranes and Porous Materials Center, Division of Physical Sciences and Engineering, King Abdullah University of Science and Technology (KAUST), Thuwal 23955-6900, Kingdom of Saudi Arabia

Supporting Information

ABSTRACT: The bottom-up assembly of nanoparticles into diverse ordered solids is a challenge because it requires nanoparticles, which are often quasi-spherical, to have interaction anisotropy akin to atoms and molecules. Typically, anisotropy has been introduced by changing the shape of the inorganic nanoparticle core. Here, we present the design, self-assembly, optical properties, and total structural determination of $Ag_{29}(BDT)_{12}(TPP)_4$, an atomically precise tetravalent nanocluster (NC) (BDT, 1,3-benzenedithiol; TPP, triphenylphosphine). It features four unique tetrahedrally symmetrical binding surface sites facilitated by the supramolecular assembly of 12 BDT (wide footprint bidentate thiols) in the ligand shell. When each of these sites was selectively functionalized by a single phosphine ligand, particle stability, synthetic yield, and the propensity to self-assemble into macroscopic crystals increased. The solid crystallized NCs have a substantially narrowed optical band gap compared to that of the solution state, suggesting strong interparticle electronic coupling occurs in the solid state.

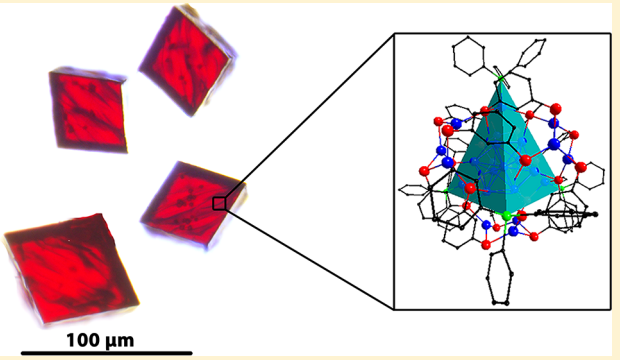

INTRODUCTION

Inspired by the diversity with which atoms and molecules form solids in nature, nanoscientists have sought to recreate their nanoparticle analogues. Efforts to design nanoparticles with interaction anisotropy analogous to atoms and molecules have mainly centered on controlling the shape of the particle's inorganic core.[1−4] Anisotropically shaped metal and semiconductor nanoparticles have successfully been assembled into large superlattices and higher-order solids.[5−9] However, this approach is inapplicable to a broad range, if not the majority, of nanoparticles, which are quasi-isotropic and highly symmetrical. For these nanoparticles, introducing anisotropy would require supramolecular engineering of the ligand shell; for example, nanoscale phase separation could be used (i.e., patchy particles)[10−12] or exploitation of topological defects that form when ligands, especially those with wide footprints, align on the three-dimensional surface of the inorganic core.[13,14] While these ligand-shell engineering approaches have shown proof-of-concept anisotropic "valences", they have not led to long-range ordered solids. The key limitation in these systems is the large disorder present in the particle's core (size and faceting), which causes a considerable variability in the configurations of the self-assembled monolayer of ligands in the shell.

There is, however, a notable class of atomically precise nanoparticles known as nanoclusters (NCs) or molecular nanoparticles[15−17] that can assemble into macroscopically ordered crystals. They typically consist of highly symmetrical inorganic cores and for stability follow electronic or geometric closing rules.[17,18] They display exotic optical and electronic properties featured by discrete molecular like energy levels,[19] size specific HOMO−LUMO gaps and photoluminescence.[20,21] Prominent examples include Au_{102},[22] Au_{25},[23,24] Ag_{44},[25−30] and most recently Au_{133}.[31,32] The vast majority of reported NCs have been synthesized with relatively small footprint ligands. Therefore, they have not been investigated for the engineering of anisotropic ligand shells, which intuition suggests would require wide footprint bidentate ligands.

Here, we present the synthesis, optical properties and structure of an atomically precise silver NC with a self-assembled monolayer of 1,3-benzenedithiol (BDT) ligands. The resulting $Ag_{29}(BDT)_{12}(TPP)_4$ NC despite being quasi-spherical, possesses four tetrahedrally symmetric positions, that can be exclusively functionalized with monodentate phosphine ligands. The selective binding of TPP ligands increases particle

Received: May 1, 2015

DOI: 10.1021/jacs.5b04547
J. Am. Chem. Soc. XXXX, XXX, XXX−XXX

stability, synthetic yield, and the tendency to self-assemble into macroscopic crystals; therefore, it was possible to elucidate their complete structure by single-crystal X-ray diffraction. A careful investigation of the structure revealed that the four tetrahedral sites formed due to the supramolecular self-assembly of a wide footprint bidentate BDT on the silver core. Phosphine ligands could functionalize these four sites selectively if introduced during synthesis or postsynthetically through ligand exchange. In its macroscopic crystallized form, the optical band gap of $Ag_{29}(BDT)_{12}(TPP)_4$ narrows substantially, indicative of enhanced interparticle electronic coupling upon NC clustering in a crystal lattice. This work demonstrates the potential of combining supramolecular engineering of the ligand shell with atomically precise metal cores to create anisotropic NC analogues of molecules that crystallize into macroscopic solids with novel collective properties.

RESULTS AND DISCUSSION

Synthesis, Purification, and Crystallization. $Ag_{29}(BDT)_{12}$ NCs were prepared by dissolving silver nitrate in a solvent solution of methanol and dichloromethane prior to the addition of BDT ligands. The solution turned turbid with insoluble yellow flakes, indicating the formation of a Ag−S complex. The reaction mixture was reduced with an aqueous solution of $NaBH_4$, and the resulting dark brown solution turned orange during 5−7 h of stirring. Supporting Information (SI) Scheme 1 shows detailed pictures of the reaction vials throughout the reaction. To purify the product, we centrifuged the solution at 9000 rpm: the products consisted of a dark brown precipitate that was discarded after failing to redisperse in other solvents and a dark orange supernatant with optical properties that indicated the presence of NCs. Figure 1 shows

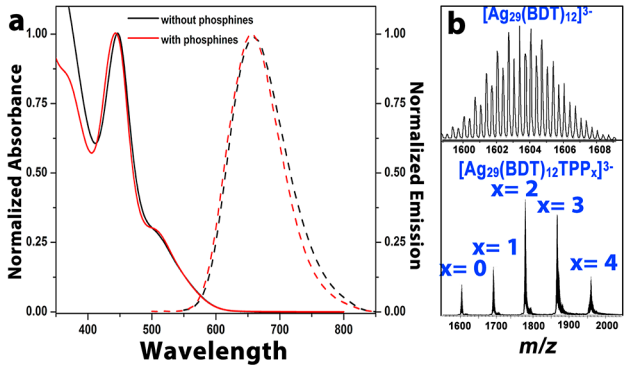

Figure 1. (a) UV−vis absorbance (solid) and emission (dashed) of $Ag_{29}(BDT)_{12}(TPP)_4$ NCs without (black) and with (red) phosphines. The excitation wavelength is at 450 nm. (b) ESI-MS of $Ag_{29}(BDT)_{12}$ without (upper panel) and with phosphines (bottom panel).

the UV−vis absorption and emission spectra of the supernatant. The as-prepared NCs exhibited molecular transitions at 447 and 513 nm and an emission maximum around 670 nm. All attempts to further purify the solution were unsuccessful as the NCs were unstable upon drying and redispersing. Using electrospray ionization mass spectrometry (ESI-MS) to further characterize these NCs, we found that $Ag_{29}(BDT)_{12}$ NCs were dominantly responsible for the peaks observed in the negative ion mode (Figure S1). The upper panel in Figure 1b shows the expansion of the 3− charged species. No added cations were used to assist in the ionization of the NCs.

We suspect that a low reaction yield (less than 0.1%) and NC instability (NCs were stable for only a couple of hours) were due to the incomplete capping of the metal surface, caused by the geometric packing limitation imposed by the wide BDT footprint. To circumvent this limitation, we incorporated different monodentate phosphine ligands in the synthesis; for example, the full reaction with TPP is depicted in SI Scheme 2. TPP was dissolved in dichloromethane and introduced to the reaction vial immediately after mixing the silver salt with BDT. The yellow flakes disappeared immediately and the solution turned clear. Eventually, a dark orange solution developed that upon centrifugation formed a pellet, which was then dried under vacuum. The purified NCs showed high solubility in various aprotic polar solvents, including DMF and DMSO, and fair solubility in less polar solvents such as acetonitrile and dichloromethane.

We performed ESI-MS to determine if the size of the NC core remained the same after functionalization with phosphine ligands and to probe the charge state of the NCs. Negative ion mode ESI-MS of the NCs in acetonitrile revealed a number of peaks in the range of m/z = 1500−2000 (Figure S2) with five sets of peaks separated by m/z = 87.5 (bottom of Figure 1b). Expansion of each peak has a characteristic isotropic distribution in which peak separation corresponds to m/z = 0.33, which in turn corresponds to the −3 charged state. Thus, the peak separation of 87.5 was assigned to the loss of one phosphine from the parent ion. Of the five peaks, the one at m/z = 1603 corresponds to $Ag_{29}(BDT)_{12}$. These results suggest the presence of four phosphines that were sequentially dissociated during ionization (a finding supported by X-ray diffraction, vide infra). The loss of phosphines during ionization is attributed to the fact that they are weakly bound to the clusters compared to thiols.[33,34] The presence of a negatively charged species of this kind, although no counterions were used to assist ionization, suggests that the nanoparticles are negatively charged. In addition, because the −3 charged state was the most abundant charged state detected, we postulate that this NC has a full molecular formula of $[Ag_{29}(BDT)_{12}(TPP)_4]^{-3}$; it follows the electron count rule of the superatom theory,[35] with an electron count of n = 29−24 + 3 = 8, corresponding to a stable superatom with the Aufbau shell filling $1S^2|1P^6|$, similar to the very stable and extensively studied $[Au_{25}(SR)_{18}]^{-1}$.[23,24]

The presence of one species in the ESI mass spectrum is an indication of the degree of uniformity of the synthesized NCs. However, there is a possibility that other species might exist that do not ionize during electrospray, and thus they will not appear in the mass spectrum. To rule out the existence of any other species, and to confirm the purity of the samples used for the measurement of the optical properties, we used analytical ultracentrifugation (AUC), a potent technique to determine the homogeneity of macromolecules and nanoclusters in solutions.[36−39] The sedimentation and diffusion distributions of the synthesized NCs in acetonitrile are shown in Figure S3. The distributions show that the NCs are highly homogeneous; at least 97% of the sample is composed of one species whose sedimentation coefficient is 2.9×10^{-13} s. The molecular weight corresponding to this most abundant species is 5381.49 Da which is in very good agreement with the mass spec assignment of $Ag_{29}(BDT)_{12}(TPP)_4$. The details of AUC technique can be found in the SI.

For crystallization, the centrifuged NCs pellet was dispersed in DMF, filtered using a syringe filter and left to evaporate

DOI: 10.1021/jacs.5b04547
J. Am. Chem. Soc. XXXX, XXX, XXX−XXX

slowly in a dark box inside a ventilated fuming hood. Within 1–2 days, self-assembled supramolecular structures had formed, as shown in Figure 2. They were obtained by drop casting onto a glass microscope slide from a concentrated stock solution; fluorescent crystals suitable for X-ray diffraction were harvested (inset of Figure 2). We used DMF as a dispersing solvent because of its high boiling point and slow evaporation time, which increased the tendency of the NCs to assemble into a large solid with a long-range order.

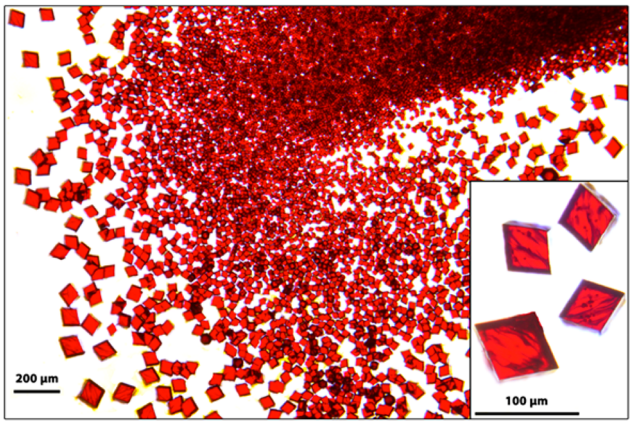

Figure 2. Optical microscopy image of self-assembled $Ag_{29}(BDT)_{12}TPP_4$ NCs. Inset shows separate rhombohedral single crystals.

X-ray Crystallography. Single crystal X-ray diffraction analysis revealed a core–shell NC with an overall composition of $Ag_{29}(BDT)_{12}(TPP)_4$, which crystallizes in a cubic *Pa*3– space group. The structure was refined to a resolution of 1.1 Å and to an R_1 value of 8.9%. $Ag_{29}(BDT)_{12}(TPP)_4$ features a centered icosahedral metal core (Figure 3a), similar to the well-known Au_{25}[23,24] and the most recently discovered Au_{133}.[31] An exterior shell (Figure 3b) composed of the remaining 16 Ag atoms caps the core.

The crystal structure reveals two types of silver atoms in the shell. Twelve silver atoms cap all the 12 atoms of the icosahedron, giving rise to four tetrahedrally oriented trigonal prisms as shown in Figure 3c. The remaining four Ag atoms face-cap the core at four tetrahedral positions (Figure 4d). Starting from the center of the icosahedron, the radial bond lengths give rise to an average of 2.77 ± 0.01 Å per Ag–Ag bond, in comparison to the 2.70 ± 0.01 Å reported for the Au–Au bonds in the Au_{13} icosahedral core of $Au_{25}(SR)_{18}$.[23,24] The average length of the peripheral Ag–Ag bonds is 2.92 ± 0.06 Å, comparable to the 2.88 Å bond length in bulk silver, indicating a strong interaction between the atoms of the core.

The shell is composed of two motifs unique to $Ag_{29}(BDT)_{12}(TPP)_4$: (i) a Ag_3S_6 crown motif (Figure 4b) where three S atoms connect the three Ag atoms of the crown in such a way that they form an alternating chair configuration and the remaining three S atoms encapsulate the underlying icosahedron face (Figure 4c); (ii) a $Ag_1S_3P_1$ motif where the S atoms connect the Ag atoms to the nearest Ag atoms and the P binds on the top site of Ag atoms (Figure 4d). It was also observed in Au NCs that phosphines prefer to bind on the top site of Au atoms.[40] Figure 4e shows that the shell composed of four Ag_3S_6 and four $Ag_1S_3P_1$ motifs provides complete passivation of the NC. Figure S4 shows how the shell is formed around the Ag_{13} core. Starting from the core (Figure S4a) outward, one S moiety of the BDT ligand is attached to each of the 12 Ag atoms of the icosahedron (Figure S4b). These S atoms bridge the core atoms to the Ag atoms in the shell. The second S moiety bridges Ag atoms in the shell (Figure S4c). The overall core–shell structure is then shown in Figure S4d highlighting two pairs of sulfurs to show which pair of sulfurs originates from a single BDT molecule.

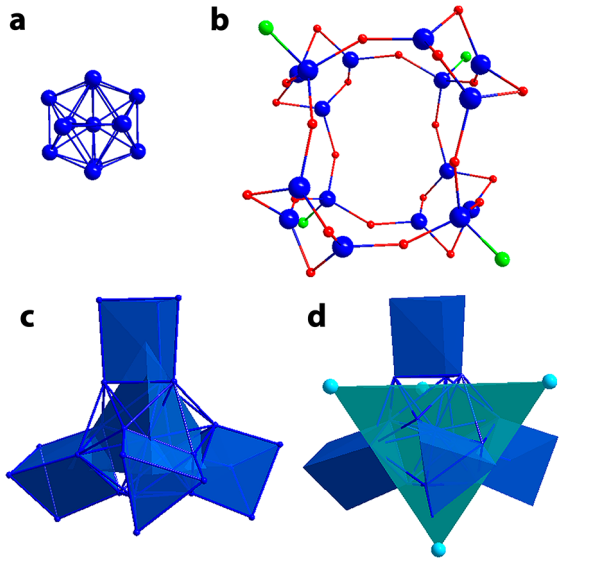

Figure 3. Anatomy of the structure of $Ag_{29}(BDT)_{12}(TPP)_4$ showing the core–shell configuration and the position of the Ag atoms: (a) Ag_{13} centered icosahedral core; (b) $Ag_{16}S_{24}P_4$ shell; (c) arrangement of 12 Ag atoms of the shell forming 4 trigonal prisms tetrahedrally oriented; (d) tetravalent sites of the NC. Color labels: Ag, blue and navy blue; S, red; P, green; all C and H atoms are omitted for clarity.

The arrangement of all the Ag atoms in the shell are influenced by the particular spacing between the two thiol groups of the ligand in addition to the high tendency of S to coordinate with Ag forcing the benzene rings to bend in such a way that all the S atoms of the bidentate ligand would coordinate to the Ag. $Ag_{29}(BDT)_{12}(TPP)_4$ is by far the first molecular NC where the underlying geometry is highly affected by the structure of the ligand. All attempts to make the NCs with similar bidentate ligands with different spacing between the two thiol groups, for example, 1,2-benzenedithiol and 1,4-benzenedithiols, failed to produce NCs stable enough for a period of time to carry any meaningful characterization, which shows how crucial is the distance between the two thiols in obtaining this tetravalent NC. Similarly, importance of the substituent position (such as –SH in our study) on the metal bound thiol in tuning cluster size was addressed by Jin's group.[41] Reversible interconversion of atomically precise silver clusters is observed in the presence of specific thiols inferring the significant role of nature of thiol ligand.[42] Interestingly, phosphines on tetravalent silver sites are labile and accessible for exchange. We demonstrated this exchange process by replacing TPP with tris(4-fluorophenyl)phosphine (TFPP). ESI-MS confirms that exchange is complete (Figure S5 in the SI). Loss of TFPP during ESI is evident from the spectrum similar to TPP. This composition was further verified by direct synthesis of TFPP functionalized $Ag_{29}(BDT)_{12}(TFPP)_4$ (Figure S6 in the SI). These mass spectral data unambiguously confirm that the functional groups on tetravalent positions are labile.

DOI: 10.1021/jacs.5b04547
J. Am. Chem. Soc. XXXX, XXX, XXX–XXX

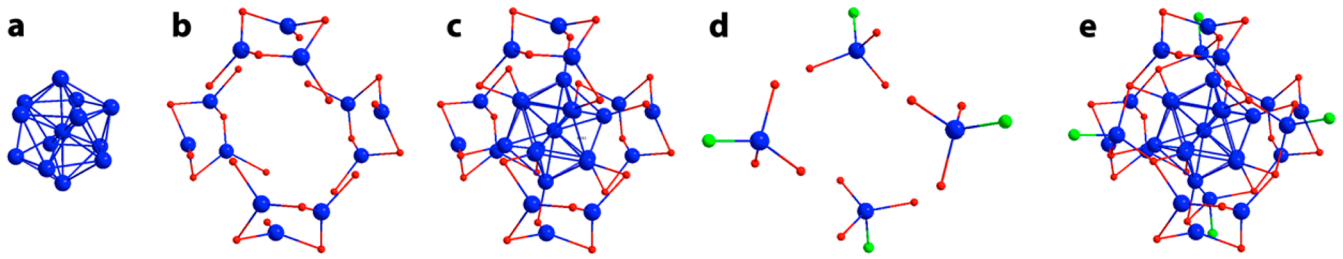

Figure 4. X-ray crystal structure of $Ag_{29}(BDT)_{12}(TPP)_4$ highlighting the two motifs present in the shell: (a) Ag_{13} centered icosahedral core; (b) $Ag_{12}S_{24}$ shell made of 4 Ag_3S_6 crowns; (c) $Ag_{25}S_{24}$ motif, where the four Ag_3S_6 crowns capping the core; (d) 4 $Ag_1S_3P_1$ motifs; (e) total structure of $Ag_{29}(BDT)_{12}(TPP)_4$. Color labels: Ag, blue; S, red; P, green; all C and H atoms are omitted for clarity.

Optical Properties. Figure 5 shows the absorption and emission spectra of $Ag_{29}(BDT)_{12}(TPP)_4$ in solution and as a

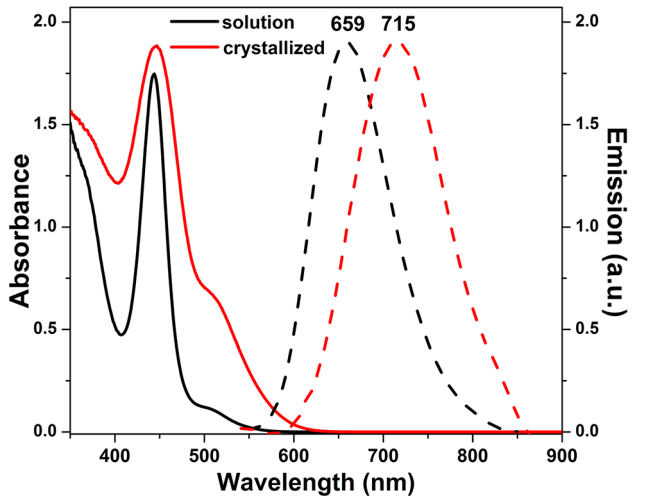

Figure 5. UV−vis absorbance (solid curves) and emission (dashed) of $Ag_{29}(BDT)_{12}(TPP)_4$ NCs in acetonitrile (black) and dried (red).

crystallized film. Upon crystallization, two main features were observed: (i) an overall increase and broadening of the long wavelength band of absorption and (ii) a red shift of the emission band by more than 50 nm. The broadening and minute red shift of the absorption band are explained in terms of electronic coupling between the NCs via interaction between the transition dipole moment of the individual absorbing $Ag_{29}(BDT)_{12}(TPP)_4$ NC and the induced dipole moments in the neighboring $Ag_{29}(BDT)_{12}(TPP)_4$ NCs. This interaction is thought to lower the initial transition energy.[43] This behavior was already observed by Zhang et al. when assembled ZnSe NCs superstructures are formed.[44] The red shift of the emission band is expected to be caused by a combined effect of the electronic coupling quoted before and of lattice-origin, nonradiative decay pathways occurring through electron−phonon interaction that lower the emission energy and also slightly broaden the emission bands. It is important to stress that when $Ag_{29}(BDT)_{12}(TPP)_4$ NCs are assembled into a crystal, a proper lattice dynamics of the superstructure, not present in isolated NCs, is generated.

DFT Calculations. To identify the origin of the optical transitions, we simulated the optical absorption of the $Ag_{29}(BDT)_{12}(TPP)_4$ NCs by the time-dependent density functional theory (see the SI for details). Despite a shift, the main peak at 450 nm and the shoulder at 520 nm from the experimental spectrum were reproduced in the simulated spectrum (Figure S7). We found that the 450 nm peak involved a transition from deep occupied orbitals (namely, HOMO−13, composed mostly of sulfur atoms' 3p states and the 4d states of Ag atoms that are directly bonded to sulfur atoms) to the LUMO+1 orbitals that corresponding to the 1D levels in the superatom theory[35] (Figure 6). One can indeed see

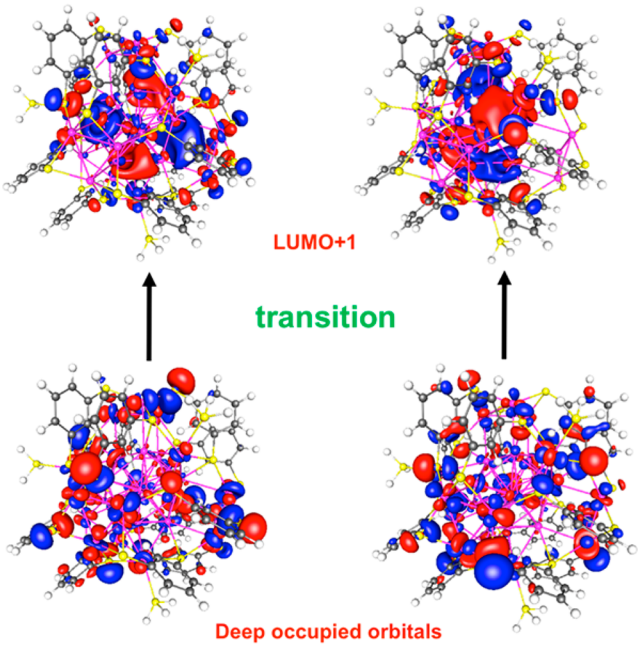

Figure 6. Orbitals that have the largest contributions to the transition responsible for the main absorption peak at 450 nm of the $Ag_{29}(BDT)_{12}(TPP)_4$ cluster (oscillator strength 0.031; see Table S1 and Figure S8 in the SI).

that the LUMO+1 orbitals show d orbital character (two nodal planes). According to TDDFT, the shoulder peak at 520 nm in Figure 5 corresponds to HOMO−10 to LUMO+1 transitions (see Figures S7−S8 and Table S1 in the SI for the orbital diagram, oscillator strength, and orbital contributions).

CONCLUSION

Using bidentate ligands, we synthesized a tetravalent $Ag_{29}(BDT)_{12}(TPP)_4$ NC, a new superatom nanoparticle, that readily assembles to form well-defined macroscopic crystals. The high stability of $Ag_{29}(BDT)_{12}(TPP)_4$, the anisotropy imparted on the ligand shell, and the modularity of the tetravalent positions make $Ag_{29}(BDT)_{12}(TPP)_4$ a good candidate as a template for future strategies to design atomically

DOI: 10.1021/jacs.5b04547
J. Am. Chem. Soc. XXXX, XXX, XXX−XXX

precise NCs with molecularly engineered anisotropies that can grow into artificially designed solids.

EXPERIMENTAL SECTION

Materials. All chemicals including silver nitrate ($AgNO_3$, 99%), benzene-1,3-dithiol (BDT, 99%), sodium borohydride ($NaBH_4$, 99.99% metals basis), triphenylphosphine (TPP, 97%), and tris(4-fluorophenyl)phosphine were purchased from Sigma-Aldrich and used without further purifications. Solvents including methanol, dichloromethane, acetone, and cyclohexane were used from Sigma as received. Distilled water (H_2O) is obtained from Milli-Q (Millipore apparatus).

Synthesis and Purification. In a 20 mL amber glass scintillation vial, 13.5 μL of BDT was added to 10 mL of DCM. A solution of 20 mg of $AgNO_3$ in 5 mL of methanol was then added to the reaction vial whereby the color of the solution turned turbid yellow, indicating the formation of the insoluble Ag−S complex. Shortly after that, a solution of 200 mg of triphenylphosphine in 1 mL of DCM was added, and the solution turned colorless, indicating the complex formation of Ag−S−P, which completely dissolves in the methanol/DCM mixture. The complex was allowed to stir for 10 min before the addition of a fresh solution of 10.5 mg of $NaBH_4$ in 500 of μL water. The color of the solution turned dark brown immediately, which gradually changed (over the course of 10−12 h) to orange, indicating the formation of the new NCs. The floating NCs were centrifuged at high speed (8000 rpm) for 2 min and collected at the bottom of the centrifuge tube. The clear supernatant was discarded, and the dark orange NCs were washed several times by ethanol to ensure the removal of all unreacted compounds. The purified NCs were left to dry overnight under vacuum.

Crystallization. The thoroughly dried powder was dispersed in 400 μL of DMF, vortexed for at least 1 min, and then filtered using a syringe filter with pore size 220 nm. The filtered sample was then spotted on microscope glass plates and left to evaporate slowly at room temperature under air in a dark box placed in a ventilated fume hood. After approximately 2 days, few square dark orange crystals were harvested.

Computational Methods. DFT Calculations of the $Ag_{29}(BDT)_{12}(TPP)_4$ cluster were performed with the quantum chemistry program Turbomole V6.5.[45] To save the computational time, we replaced phenyl rings on TPP ligands with −H groups; in other words, we simulated $[Ag_{29}(BDT)_{12}(PH_3)_4]^{3-}$. This is a commonly employed approximation, which we think is valid here, given that the Ph− groups on TPP are not involved in the frontier orbitals of the cluster. The def2-SV(P) basis sets were used for C, P, S, and H, while effective core potentials which have 19 valence electrons and include scalar relativistic corrections were used for Ag.[46] Geometry optimization was done with the TPSS (Tao, Perdew, Staroverov, and Scuseria) functional.[47] Time-dependent DFT calculations were done at the PBE level. All transitions together with their oscillator strengths were then convoluted with a Lorentzian line shape of 0.15 eV broadening to make the optical-absorption spectrum.

ASSOCIATED CONTENT

Supporting Information

Instrumentation, synthesis schemes, ESI-MS spectra, and crystal structural data. CCDC number is 1056509. The Supporting Information is available free of charge on the ACS Publications website at DOI: 10.1021/jacs.5b04547.

AUTHOR INFORMATION

Corresponding Author

*osman.bakr@kaust.edu.sa

Notes

The authors declare no competing financial interest.

ACKNOWLEDGMENTS

The authors acknowledge the use of KAUST's Core Laboratories. The computational work was supported by the University of California, Riverside.

REFERENCES

(1) Glotzer, S. C.; Solomon, M. J. *Nat. Mater.* **2007**, *6*, 557.
(2) Schmid, G. *Nanoparticles: from theory to application*; John Wiley & Sons: Weinheim, Germany, 2011.
(3) Fedlheim, D. L.; Foss, C. A. *Metal nanoparticles: synthesis, characterization, and applications*; CRC Press: Boca Raton, FL, 2001.
(4) Jackson, A. M.; Myerson, J. W.; Stellacci, F. *Nat. Mater.* **2004**, *3*, 330.
(5) Pileni, M.-P. *Acc. Chem. Res.* **2007**, *40*, 685.
(6) Talapin, D. V.; Lee, J.-S.; Kovalenko, M. V.; Shevchenko, E. V. *Chem. Rev.* **2010**, *110*, 389.
(7) Manna, L.; Scher, E. C.; Alivisatos, A. P. *J. Am. Chem. Soc.* **2000**, *122*, 12700.
(8) Malikova, N.; Pastoriza-Santos, I.; Schierhorn, M.; Kotov, N. A.; Liz-Marzán, L. M. *Langmuir* **2002**, *18*, 3694.
(9) Lee, S. H.; Yu, S.-H.; Lee, J. E.; Jin, A.; Lee, D. J.; Lee, N.; Jo, H.; Shin, K.; Ahn, T.-Y.; Kim, Y.-W.; Choe, H.; Sung, Y.-E.; Hyeon, T. *Nano Lett.* **2013**, *13*, 4249.
(10) DeVries, G. A.; Brunnbauer, M.; Hu, Y.; Jackson, A. M.; Long, B.; Neltner, B. T.; Uzun, O.; Wunsch, B. H.; Stellacci, F. *Science* **2007**, *315*, 358.
(11) Zhang, G.; Wang, D.; Möhwald, H. *Angew. Chem., Int. Ed.* **2005**, *44*, 7767.
(12) Zhang, Z.; Keys, A. S.; Chen, T.; Glotzer, S. C. *Langmuir* **2005**, *21*, 11547.
(13) Nelson, D. R. *Nano Lett.* **2002**, *2*, 1125.
(14) Wang, Y.; Wang, Y.; Breed, D. R.; Manoharan, V. N.; Feng, L.; Hollingsworth, A. D.; Weck, M.; Pine, D. J. *Nature* **2012**, *491*, 51.
(15) Whetten, R. L.; Khoury, J. T.; Alvarez, M. M.; Murthy, S.; Vezmar, I.; Wang, Z. L.; Stephens, P. W.; Cleveland, C. L.; Luedtke, W. D.; Landman, U. *Adv. Mater.* **1996**, *8*, 1521.
(16) Niihori, Y.; Matsuzaki, M.; Pradeep, T.; Negishi, Y. *J. Am. Chem. Soc.* **2013**, *135*, 4946.
(17) Maity, P.; Xie, S.; Yamauchi, M.; Tsukuda, T. *Nanoscale* **2012**, *4*, 4027.
(18) Häkkinen, H. *Nat. Chem.* **2012**, *4*, 443.
(19) Chen, S.; Ingram, R. S.; Hostetler, M. J.; Pietron, J. J.; Murray, R. W.; Schaaff, T. G.; Khoury, J. T.; Alvarez, M. M.; Whetten, R. L. *Science* **1998**, *280*, 2098.
(20) Wang, S.; Meng, X.; Das, A.; Li, T.; Song, Y.; Cao, T.; Zhu, X.; Zhu, M.; Jin, R. *Angew. Chem., Int. Ed.* **2014**, *53*, 2376.
(21) Yu, Y.; Luo, Z.; Chevrier, D. M.; Leong, D. T.; Zhang, P.; Jiang, D.-e.; Xie, J. *J. Am. Chem. Soc.* **2014**, *136*, 1246.
(22) Jadzinsky, P. D.; Calero, G.; Ackerson, C. J.; Bushnell, D. A.; Kornberg, R. D. *Science* **2007**, *318*, 430.
(23) Heaven, M. W.; Dass, A.; White, P. S.; Holt, K. M.; Murray, R. W. *J. Am. Chem. Soc.* **2008**, *130*, 3754.
(24) Zhu, M.; Aikens, C. M.; Hollander, F. J.; Schatz, G. C.; Jin, R. *J. Am. Chem. Soc.* **2008**, *130*, 5883.
(25) Desireddy, A.; Conn, B. E.; Guo, J.; Yoon, B.; Barnett, R. N.; Monahan, B. M.; Kirschbaum, K.; Griffith, W. P.; Whetten, R. L.; Landman, U.; Bigioni, T. *Nature* **2013**, *501*, 399.
(26) Yang, H.; Wang, Y.; Huang, H.; Gell, L.; Lehtovaara, L.; Malola, S.; Häkkinen, H.; Zheng, N. *Nat. Commun.* **2013**, *4*, 2422.
(27) AbdulHalim, L. G.; Ashraf, S.; Katsiev, K.; Kirmani, A. R.; Kothalawala, N.; Anjum, D. H.; Abbas, S.; Amassian, A.; Stellacci, F.; Dass, A.; Hussain, I.; Bakr, O. M. *J. Mater. Chem. A* **2013**, *1*, 10148.
(28) Bakr, O. M.; Amendola, V.; Aikens, C. M.; Wenseleers, W.; Li, R.; Dal Negro, L.; Schatz, G. C.; Stellacci, F. *Angew. Chem.* **2009**, *121*, 6035.
(29) Harkness, K. M.; Tang, Y.; Dass, A.; Pan, J.; Kothalawala, N.; Reddy, V. J.; Cliffel, D. E.; Demeler, B.; Stellacci, F.; Bakr, O. M.; McLean, J. A. *Nanoscale* **2012**, *4*, 4269.

DOI: 10.1021/jacs.5b04547
J. Am. Chem. Soc. XXXX, XXX, XXX−XXX

(30) AbdulHalim, L. G.; Kothalawala, N.; Sinatra, L.; Dass, A.; Bakr, O. M. *J. Am. Chem. Soc.* **2014**, *136*, 15865.
(31) Dass, A.; Theivendran, S.; Nimmala, P. R.; Kumara, C.; Jupally, V. R.; Fortunelli, A.; Sementa, L.; Barcaro, G.; Zuo, X.; Noll, B. C. *J. Am. Chem. Soc.* **2015**, *137*, 4610.
(32) Zeng, C.; Chen, Y.; Kirschbaum, K.; Appavoo, K.; Sfeir, M. Y.; Jin, R. *Sci. Adv.* **2015**, *1*, e1500045.
(33) Yanagimoto, Y.; Negishi, Y.; Fujihara, H.; Tsukuda, T. *J. Phys. Chem. B* **2006**, *110*, 11611.
(34) Das, A.; Li, T.; Nobusada, K.; Zeng, Q.; Rosi, N. L.; Jin, R. *J. Am. Chem. Soc.* **2012**, *134*, 20286.
(35) Walter, M.; Akola, J.; Lopez-Acevedo, O.; Jadzinsky, P. D.; Calero, G.; Ackerson, C. J.; Whetten, R. L.; Grönbeck, H.; Häkkinen, H. *Proc. Natl. Acad. Sci. U. S. A.* **2008**, *105*, 9157.
(36) Carney, R. P.; Kim, J. Y.; Qian, H.; Jin, R.; Mehenni, H.; Stellacci, F.; Bakr, O. M. *Nat. Commun.* **2011**, *2*, 335.
(37) Sousa, A. A.; Morgan, J. T.; Brown, P. H.; Adams, A.; Jayasekara, M.; Zhang, G.; Ackerson, C. J.; Kruhlak, M. J.; Leapman, R. D. *Small* **2012**, *8*, 2277.
(38) Harkness, K. M.; Tang, Y.; Dass, A.; Pan, J.; Kothalawala, N.; Reddy, V. J.; Cliffel, D. E.; Demeler, B.; Stellacci, F.; Bakr, O. M. *Nanoscale* **2012**, *4*, 4269.
(39) Demeler, B.; Nguyen, T.-L.; Gorbet, G. E.; Schirf, V.; Brookes, E. H.; Mulvaney, P.; El-Ballouli, A. a. O.; Pan, J.; Bakr, O. M.; Demeler, A. K.; Uribe, B. I. H.; Bhattarai, N.; Whetten, R. L. *Anal. Chem.* **2014**, *86*, 7688.
(40) Shichibu, Y.; Negishi, Y.; Watanabe, T.; Chaki, N. K.; Kawaguchi, H.; Tsukuda, T. *J. Phys. Chem. C* **2007**, *111*, 7845.
(41) Chen, Y.; Zeng, C.; Kauffman, D. R.; Jin, R. *Nano Lett.* **2015**, *15*, 3603.
(42) Bootharaju, M. S.; Burlakov, V. M.; Besong, T. M.; Joshi, C. P.; AbdulHalim, L. G.; Black, D.; Whetten, R.; Goriely, A.; Bakr, O. M. *Chem. Mater.* **2015**, *27*, 4289−4297.
(43) Döllefeld, H.; Weller, H.; Eychmüller, A. *J. Phys. Chem. B* **2002**, *106*, 5604.
(44) Zhang, J.; Rowland, C.; Liu, Y.; Xiong, H.; Kwon, S.; Shevchenko, E.; Schaller, R. D.; Prakapenka, V. B.; Tkachev, S.; Rajh, T. *J. Am. Chem. Soc.* **2015**, *137*, 742.
(45) Ahlrichs, R.; Bär, M.; Häser, M.; Horn, H.; Kölmel, C. *Chem. Phys. Lett.* **1989**, *162*, 165.
(46) Andrae, D.; Haeussermann, U.; Dolg, M.; Stoll, H.; Preuss, H. *Theor. Chim. Acta* **1990**, *77*, 123.
(47) Tao, J.; Perdew, J. P.; Staroverov, V. N.; Scuseria, G. E. *Phys. Rev. Lett.* **2003**, *91*, 146401.

DOI: 10.1021/jacs.5b04547
J. Am. Chem. Soc. XXXX, XXX, XXX−XXX